ON-LINE APPENDIX

The CFD ABO Study Group Member List

Principal Investigator. Shunichi Fukuda, MD, PhD, Department of Neurosurgery, Kyoto Medical Center.

Representative for CFD Analysis. Yuji Shimogonya, PhD, College of Engineering, Nihon University.

Representative for Statistical Analysis. Naohiro Yonemoto, MPH, Department of Biostatistics, Kyoto University.

Representatives of Participating Institutes. Tetsuya Tsukahara, MD, PhD, Department of Neurosurgery, Kyoto Medical Center; Yasushi Okada, MD, PhD, Department of Cerebrovascular Disease and Neurology, Kyushu Medical Center; Keisuke Tsutsumi, MD, PhD, Department of Neurosurgery, Nagasaki Medical Center; Noriyuki Suzaki, MD, PhD, Department of Neurosurgery, Nagoya Medical Center; Noriyuki Kato, MD, PhD, Department of Neurosurgery, Mito Medical Center; Kentaro Kawarabuki, MD, PhD, Department of Neurosurgery, Maizuru Medical Center; Masayuki Ishihara, MD, PhD, Department of Neurosurgery, Tochigi Medical Center; Sadahiro Maejima, MD, PhD, Department of Neurosurgery, Saitama National Hospital; Ryoichi Saito, MD, PhD, Department of Neurosurgery, Kanagawa National Hospital; Takashi Sadatomo, MD, PhD, Department of Neurosurgery, Higashihirosima Medical Center; Yoshinari Nakamura, MD, PhD, Department of Neurosurgery, Minami Wakayama Medical Center; Eiichirou Urasaki, MD, PhD, Department of Neurosurgery, Nagasaki Kawatana Medical Center; Masayuki Miyazono, MD, PhD, Department of Neurosurgery, Ureshino Medical Center; Osamu Narumi, MD, PhD, Department of Neurosurgery, Himeji Medical Center; Keiichi Sakai, MD, PhD, Department of Neurosurgery, Shinshu Ueda Medical Center; Katsuo Shoin, MD, PhD, Department of Neurosurgery, Kanazawa Medical Center; Hidehiro Hirabayashi, MD, PhD, Department of Neurosurgery, Nara Medical Center; Tadahiro Otsuka, MD, PhD, Department of Neurosurgery, Kumamoto Medical Center; Junichi Imamura, MD, PhD, Department of Neurosurgery, Kagoshima Medical Center; Katsuhiro Yamashita, MD, PhD, Department of Neurosurgery, Kanmon Medical Center; Hiroyuki Masaoka, MD, PhD, Department of Neurosurgery, Disaster Medical Center; Shinji Ooba, MD, PhD, Department of Neurosurgery, Kure Medical Center; Takahito Nakajo, MD, PhD, Department of Neurosurgery, Kochi National Hospital; Yasuyuki Nagai, MD, PhD, Department of Neurosurgery, Beppu Medical Center; Tomonori Yamada, MD, PhD, Department of Neurosurgery, Osaka Minami Medical Center.

Assistant Investigators for CFD Analysis. Naoko Hayakawa, RN, School of Nursing and Midwifery, Kyoto Medical Center; Miyuki Fukuda, MD, PhD, Clinical Research Institute, National Hospital Organization Kyoto Medical Center; Yasuhide Imoto, MS, Graduate School of Engineering, University of Hyogo.

Secretaries. Natsuko Nakajo, Department of Neurosurgery, Kyoto Medical Center; Satomi Kikuchi, Department of Neurosurgery, Kyoto Medical Center; Kazuha Fujiwara, Department of Neurosurgery, Kyoto Medical Center.

The CFD ABO Study

To examine details of the hemodynamics in human cerebral aneurysms and to clarify hemodynamic risk factors for the development, enlargement, and rupture of cerebral aneurysms with computational fluid dynamics techniques, we initiated the multiinstitutional prospective observational clinical study the Computational Fluid Dynamics Analysis of Blood Flow in Cerebral Aneurysms: Prospective Observational Study (the CFD ABO study) as a National Hospital Organization collaborative clinical study (UMIN000013584). The study was approved by the Ethics Committee of the Kyoto Medical Center, Japan. It is being conducted at 25 institutions (see the Member List at left), and 461 cases were registered during a 2-year registration period (from April 1, 2014, to March 31, 2016). The study was in an observation phase until March 31, 2019. In addition to patient-specific 3D arterial geometry, actual flow velocities were measured using a carotid sonography Doppler technique to provide patient-specific physiologic data. A flow chart of the methods used in this study is shown in On-line Fig 1.

CFD Modeling. Patient-specific vascular models of the aneurysms and connected vessels were reconstructed from the corresponding 3D CTA images using Mimics and 3-matic (Materialise, Leuven, Belgium). Computational meshes of tetrahedron elements with wall boundary–fitted prism elements (5 layers in total) were generated with a resolution of 0.15–0.2 mm for each vascular model using the Mixed-Element Grid Generator in 3D (MEGG3D).[1,2] The total numbers of mesh elements ranged from approximately 5 to 10 million, depending on the cases. Pulsatile blood flow was simulated using a CFD software package, ANSYS CFX (ANSYS). Individual peak-systolic and end-diastolic velocities and vessel diameters were measured with the Doppler sonography technique on both ICAs of each patient to calculate the corresponding flow rates. A pulsatile flow rate waveform of the ICA derived from the literature[3] was scaled to the calculated peak-systolic and end-diastolic mean flow rates to impose the CFD inlet (ICA) boundary conditions. For the outlet boundary conditions, flow-rate divisions consistent with the Murray principle of minimal work[4] were prescribed. The wall was assumed to be rigid, and blood was treated as a Newtonian fluid with a density of 1050 kg/m^3 and a viscosity of 0.0035 Pa · s, because the elastic material properties of vessel walls and non-Newtonian viscous nature of blood are thought to be a second-order effect compared with geometric differences and choice of inlet boundary conditions.[5]

Hemodynamic Metrics. In the present study, we calculated the following 7 hemodynamic metrics with special attention to WSS magnitude and temporal disturbance: OSI, GON, and NtransWSS.

WSS Magnitude–Based Metrics. The WSS magnitude–based metrics considered in the present study included TAWSS, NWSS, TAWSSG, and NWSSG.

TAWSS was calculated by integrating the magnitude of the WSS, $|\vec{\tau}_w|$, at each node over the cardiac cycle T:

$$1) \qquad \mathrm{TAWSS} = \frac{1}{T}\int_0^T |\vec{\tau}_w| dt.$$

To allow comparison among different patients, we calculated the NWSS by dividing the nodal TAWSS by the fully developed TAWSS value at the ICA ($TAWSS_{ICA}$) of the same patient, which was calculated on the basis of the mean diameter and imposed cycle-averaged flow rate at the ICA of the same patient and the assumed viscosity:

$$2) \qquad NWSS = \frac{TAWSS}{TAWSS_{ICA}}.$$

The TAWSSG was computed by integrating the WSS gradient (WSSG) magnitude $|\vec{G}_w|$ at each node over the cardiac cycle T:

$$3) \qquad TAWSSG = \frac{1}{T}\int_0^T |\vec{G}_w| dt,$$

where $\vec{G}_w$ is the WSSG vector based on the definition by Lei et al[6] For the same purpose as NWSS, the NWSSG was also computed by using the nodal TAWSSG, $TAWSS_{ICA}$, and the mean diameter at the ICA (D_{ICA}) as follows:

$$4) \qquad NWSSG = \frac{TAWSSG}{TAWSS_{ICA}/D_{ICA}}.$$

WSS Disturbance–Based Metrics. The WSS disturbance–based metrics that we considered in the present study included OSI,[7] GON,[8] and NtransWSS. These metrics were computed to evaluate the intensity of the temporal disturbance of WSS or WSSG during the cardiac cycle.

OSI, a metric for characterizing the change in the WSS magnitude and direction, was defined as follows:

$$5) \qquad OSI = \frac{1}{2}\left(1 - \frac{\left|\int_0^T \vec{\tau}_w dt\right|}{\int_0^T |\vec{\tau}_w| dt}\right).$$

The GON, a metric to characterize the change in the WSSG magnitude and direction, was defined as follows:

$$6) \qquad GON = 1 - \frac{\left|\int_0^T \vec{G}_w dt\right|}{\int_0^T |\vec{G}_w| dt}.$$

In 2013, Peiffer et al[9] proposed the transverse WSS (transWSS), which can quantify the multidirectional disturbance of WSS in a different way from the OSI, by integrating the magnitude of WSS components acting transverse to the cycle-averaged WSS direction over the cardiac cycle. In the present study, we defined a new metric, NtransWSS, by dividing the nodal transWSS by the TAWSS at the same node, which allows comparison among different patients:

$$7) \qquad NtransWSS = \frac{\int_0^T |\vec{\tau}_w \cdot \vec{m}_w| dt}{\int_0^T |\vec{\tau}_w| dt},$$

where $\vec{m}_w$ is the unit vector perpendicular to both the cycle-averaged WSS direction and the normal direction of the wall surface.

OSI, GON, and NtransWSS are all nondimensional metrics, ranging from 0 to 0.5, from 0 to 1, and from 0 to 1, respectively. TAWSS, NWSS, TAWSSG, NWSSG, OSI, GON, and NtransWSS were further averaged over the aneurysm surface to allow aneurysm-specific statistical comparison among the different patients, where the aneurysm neck was interactively delineated as seen in Cebral et al[10] (On-line Fig 2).

Geometric Parameters. The following 9 geometric parameters of the aneurysm were calculated to examine the correlation between the hemodynamic and geometric parameters: size, surface area, volume, parent artery diameter, size ratio (size divided by parent artery diameter), area ratio (surface area divided by parent artery cross-section area), aspect ratio (height divided by neck width), aspect ratio × size ratio, and AAI. The AAI, a newly proposed metric to characterize the nonsphericity of aneurysmal shapes, was defined as:

$$8) \qquad AAI = \text{Aspect Ratio} \times \text{Asphericity} = \frac{H}{N} \times \frac{d^2}{S},$$

where H is height, N is neck width, d is size, and S is surface area.

Risk-Factor Selection for Multivariate Analyses. In the present study, we selected 6 risk factors for cerebral aneurysm rupture: size (maximum diameter of the cerebral aneurysm), location, sex, age (70 years or older), history of hypertension, and smoking. Greving et al[11] analyzed cumulative rupture rates with Kaplan-Meier curves and assessed predictors with Cox proportional hazard regression analysis using 8382 participants in 6 prospective cohort studies and proposed the Population, Hypertension, Age, Size of Aneurysm, Earlier Subarachnoid Hemorrhage from Another Aneurysm, and Site of Aneurysm (PHASES) aneurysm risk score. The PHASES score includes population, history of hypertension, age (70 years or older), size, earlier SAH from another aneurysm, and location. Among them, we selected hypertension, age (70 years or older), size, and location. Because the present clinical study was conducted only in Japan, we did not use "population" as a risk factor. We also did not include "earlier SAH from another aneurysm" among the risk factors for multivariate analyses because such patients may have genetic diseases in which cerebral arteries become vulnerable, leading to different hemodynamic responses. Smoking and sex (female) are also reported as independent risk factors for SAH.[12,13]

REFERENCES

1. Ito Y, Nakahashi K. **Direct surface triangulation using stereolithography data.** *AIAA Journal* 2002;40:490–96 CrossRef
2. Ito Y, Shih AM, Soni BK, et al. **Multiple marching direction approach to generate high quality hybrid meshes.** *AIAA Journal* 2007; 45:162–67 CrossRef

3. Valencia A, Morales H, Rivera R, et al. **Blood flow dynamics in patient-specific cerebral aneurysm models: the relationship between wall shear stress and aneurysm area index.** *Med Eng Phys* 2008;30:329–40 CrossRef Medline
4. Murray CD. **The physiological principle of minimum work. I: the vascular system and the cost of blood volume.** *Proc Natl Acad Sci U S A* 1926;12:207–14 CrossRef Medline
5. Cebral JR, Castro MA, Appanaboyina S, et al. **Efficient pipeline for image-based patient-specific analysis of cerebral aneurysm hemodynamics: technique and sensitivity.** *IEEE Trans Med Imaging* 2005;24:457–67 CrossRef Medline
6. Lei M, Giddens DP, Jones SA, et al. **Pulsatile flow in an end-to-side vascular graft model: comparison of computations with experimental data.** *J Biomech Eng* 2001;123:80–87 CrossRef Medline
7. He X, Ku DN. **Pulsatile flow in the human left coronary artery bifurcation: average conditions.** *J Biomech Eng* 1996;118:74–82 CrossRef Medline
8. Shimogonya Y, Ishikawa T, Imai Y, et al. **Can temporal fluctuation in spatial wall shear stress gradient initiate a cerebral aneurysm? A proposed novel hemodynamic index, the gradient oscillatory number (GON).** *J Biomech* 2009;42:550–54 CrossRef Medline
9. Peiffer V, Sherwin SJ, Weinberg PD. **Computation in the rabbit aorta of a new metric: the transverse wall shear stress—to quantify the multidirectional character of disturbed blood flow.** *J Biomech* 2013;46:2651–58 CrossRef Medline
10. Cebral JR, Mut F, Weir J, et al. **Quantitative characterization of the hemodynamic environment in ruptured and unruptured brain aneurysms.** *AJNR Am J Neuroradiol* 2011;32:145–51 CrossRef Medline
11. Greving JP, Wermer M, Brown RD Jr, et al. **Development of the PHASES score for prediction of risk of rupture of intracranial aneurysms: a pooled analysis of six prospective cohort studies.** *Lancet Neurol* 2014;13:59–66 CrossRef Medline
12. Shinton R, Beevers G. **Meta-analysis of relation between cigarette smoking and stroke.** *BMJ* 1989;298:789–94 CrossRef Medline
13. Lindekleiv H, Sandvei MS, Njølstad I, et al. **Sex differences in risk factors for aneurysmal subarachnoid hemorrhage: a cohort study.** *Neurology* 2011;76:637–43 CrossRef Medline

On-line Table 1: Associations of hemodynamic metrics—the size and location of cerebral aneurysms as assessed by multivariate logistic analysis and associations of the size and location of cerebral aneurysms. Hemodynamic metrics as assessed by multivariate regression analysis after adjustment for age (70 years or older), sex, hypertension, smoking history, and location (AcomA and MCA aneurysms) or size[a]

Dependent Variable	Independent Variable								
	AcomA	Size	TAWSS	NWSS	TAWSSG	NWSSG	OSI	GON	NtransWSS
AcomA									
OR (1/OR)			0.824 (1.213)	0.819 (1.222)	0.861 (1.162)	0.866 (1.154)	1.073	1.083	1.275[c]
95% CI			0.720–0.915	0.708–0.914	0.768–0.937	0.776–0.942	0.979–1.192	0.969–1.229	1.020–1.639
P value			<.0001[b]	<.0001[b]	<.0001[b]	<.0001[b]	.1336	.1641	.0320[b]
Size ≥7 mm									
OR (1/OR)			0.877 (1.140)	0.877 (1.140)	0.796 (1.256)	0.864 (1.157)	1.189	1.282	1.579[c]
95% CI			0.747–0.980	0.747–0.980	0.640–0.928	0.747–0.961	1.079–1.341	1.126–1.512	1.238–2.128
P value			.0146[b]	.0146[b]	.0005[b]	.0020[b]	.0002[b]	<.0001[b]	<.0001[b]
TAWSS									
β	−1.82	−0.561							
95% CI	−2.84 to −0.80	−1.064 to −0.058							
P value	.0007[b]	.0294[b]							
NWSS									
β	−2.45	−0.867							
95% CI	−3.75 to −1.15	−1.510 to −0.224							
P value	.0004[b]	.0089[b]							
TAWSSG									
β	−2.05	−0.868							
95% CI	−3.31 to −0.80	−1.486 to −0.249							
P value	.0017[b]	.0066[b]							
NWSSG									
β	−6.91	−3.22							
95% CI	−10.84 to −2.98	−5.16 to −1.28							
P value	.0008[b]	.0014[b]							
OSI									
β	0.00207	0.00332							
95% CI	−0.00078–0.00492	0.00191–0.00472							
P value	.152	<.0001[b]							
GON									
β	0.00658	0.0145							
95% CI	−0.00319–0.01634	0.0097–0.0193							
P value	.1839	<.0001[b]							
NtransWSS									
β	.0119	.0145							
95% CI	0.0006–0.0232	0.0089–0.0200							
P value	.0394[b]	<.0001[b]							

[a] Before we performed the multivariate logistic analysis, each variable was divided by 1/5 of the median value so that it was easy to compare the OR between each variable.

[b] $P < .05$.

[c] The highest OR.

On-line Table 2: Associations of aneurysmal arterial geometric parameters–hemodynamic metrics[a]

Arterial Geometric Parameters	TAWSS	NWSS	TAWSSG	NWSSG	OSI	GON	NtransWSS
Size							
β	−0.561	−0.867	−0.868	−3.22	0.00332	0.0145	0.0145
95% CI	−1.064 to −0.058	−1.510 to −0.224	−1.486 to −0.249	−5.16 to −1.28	0.00191–0.00472	0.0097–0.0193	0.0089–0.0200
P value	.02[b]	.008[b]	.006[b]	.001[b]	<.001[b]	<.001[b]	<.001[b]
Surface area							
β	−0.0241	−0.0332	−0.0353	−0.117	0.000147	0.000606	0.000638
95% CI	−0.0472 to −0.0009	−0.0631 to −0.0033	−0.0639 to −0.0066	−0.208 to −0.026	0.000082–0.000212	0.000376–0.000835	0.000379–0.000896
P value	.04[b]	.03[b]	.01[b]	.01[b]	<.001[b]	<.001[b]	<.001[b]
Volume							
β	−0.0193	−0.0261	−0.0289	−0.0922	0.000133	0.000571	0.000574
95% CI	−0.0407–0.002	−0.0537–0.0015	−0.0553 to −0.0024	−0.1766 to −0.078	0.000074–0.000193	0.000364–0.000780	0.000336–0.000812
P value	.07	.06	.03[b]	.03[b]	<.001[b]	<.001[b]	<.001[b]
Parent artery diameter							
β	−0.0167	0.467	−0.638	4.56[c]	−0.00315	−0.00877	−0.0105
95% CI	−2.0157–2.0491	−2.163–3.097	−3.175–1.899	−3.49 to −12.60	−0.00935–0.00305	−0.03152–0.01399	−0.0357–0.0147
P value	.98	.72	.61	.26	.31	.44	.40
Size ratio							
β	−0.891[c]	−1.44[c]	−1.24[c]	−6.03[c]	0.00676[c]	0.0274[c]	0.00226
95% CI	−1.884–0.101	−2.71 to −0.17	−2.47 to −0.003	−9.84 to −2.23	0.00405–0.00947	0.0128–0.0369	0.00144–0.0308
P value	.07	.02[b]	.04[b]	.002[b]	<.001[b]	<.001[b]	<.001[b]
Area ratio							
β	−0.0639	−0.0866	−0.0836	−0.348	0.000545	0.00203	0.00181
95% CI	−0.1400–0.0122	−0.1850–0.0118	−0.1786–0.0114	−0.0647 to −0.0487	0.000342–0.000749	0.00089–0.00253	0.00098–0.00265
P value	.09	.08	.08	.02[b]	<.001[b]	<.001[b]	<.001[b]
Aspect ratio							
β	−2.46[c]	−3.20	−2.92[c]	−10.5[c]	0.00799[c]	0.0352[c]	0.0379[c]
95% CI	−5.12–0.21	−6.65–0.25	−6.26–0.42	−21.1–0.2	−0.00017–0.01616	0.0057–0.0648	0.0052–0.0707
P value	.07	.06	.08	.05	.05	.02[b]	.02[b]
Aspect ratio/size ratio							
β	−0.632[c]	−0.854[c]	−0.770	−3.09	0.00329	0.0131	0.0144
95% CI	−1.20 to −0.06	−1.588 to −0.121	−1.481 to −0.058	−5.32 to −0.86	0.00165–0.00493	0.0072–0.0190	0.0079–0.0209
P value	.02[b]	.02[b]	.03[b]	.007[b]	<.001[b]	<.001[b]	<.001[b]
Aspect ratio–asphericity index							
β	−4.02[c]	−5.46[c]	−4.72[c]	−17.3[c]	0.0121[c]	0.0559[c]	0.0558[c]
95% CI	−8.23–0.19	−10.90 to −0.01	−9.99–0.56	−34.0 to −0.5	−0.0008–0.0250	0.0092–0.1027	0.0038–0.1079
P value	.06	.04[b]	.07[b]	.04[b]	.06	.01[b]	.03[b]

[a] Multivariate regression analysis after adjustment for age (70 years or older), sex, hypertension, smoking history, location (AcomA and MCA aneurysms), and each arterial geometric parameter.

[b] $P < .05$.

[c] $|\beta|$ > the value of regression coefficient in size.

On-line Table 3: Differences in flow rate in parent vessels and size between anterior communicating artery (AcomA) and MCA aneurysms[a]

	Flow Rate in Parent Vessel (mL/min)	Size (mm)
AcomA	90.9 ± 41.9	5.82 ± 2.10
MCA	123.0 ± 50.9	5.46 ± 2.00
P value	<.001[b]	.37

[a] Continuous data are presented as mean ± SD.
[b] $P < .05$, Wilcoxon rank sum test.

On-line Table 4: Differences in flow rate in parent vessels and size between larger and smaller size groups[a]

Aneurysm Size	Flow Rate in Parent Vessel (mL/min)	Size (mm)
<7 mm	112.8 ± 50.8	4.58 ± 1.71
≥7 mm	92.2 ± 41.9	8.28 ± 1.16
P value	.16	<.001[b]

[a] Continuous data are presented as mean ± SD.
[b] $P < .05$, Wilcoxon rank sum test.

On-line Table 6: Flow rate and TAWSS on the ICA in MCA aneurysm cases[a]

Aneurysm Size	ICA Flow Rate (mL/min)	TAWSS on ICA (Pa)
<5 mm	48.7 ± 15.9	0.698 ± 0.274
≥5 mm	64.1 ± 23.1	0.957 ± 0.357
P value	.03[b]	.03[b]

[a] Continuous data are presented as mean ± SD.
[b] $P < .05$, Wilcoxon rank sum test.

On-line Table 5: Differences in hemodynamic metrics between 2 different size groups with a threshold of 5 or 7 mm[a]

Threshold	TAWSS	NWSS	TAWSSG	NWSSG	OSI	GON	NtransWSS
Size (5 mm)							
β	−1.27	−2.37	−1.89	−7.97	0.00367	0.0207	0.0176
95% CI	−2.74–0.69	−3.66 to −1.08	−3.17 to −0.61	−11.87 to −4.06	0.00046–0.00688	0.0096–0.0319	0.0047–0.0304
P value	.01[b]	<.001[b]	.004[b]	<.001[b]	.02[b]	<.001[b]	.007[b]
Size (7 mm)							
β	−1.20	−1.48	−1.70	−5.20	0.00648	0.0260	0.0274
95% CI	−2.33 to −0.08	−2.95 to −0.02	−3.10 to −0.31	−9.68 to −0.73	0.00323–0.00973	0.0143–0.0376	0.0144–0.0404
P value	.03[b]	.04[b]	.01[b]	.02[b]	<.001[b]	<.001[b]	<.001[b]

[a] Multivariate regression analysis after adjustment for age (70 years or older), sex, hypertension, smoking history, location (AcomA and MCA aneurysms), and size (5 or 7 mm).
[b] $P < .05$.

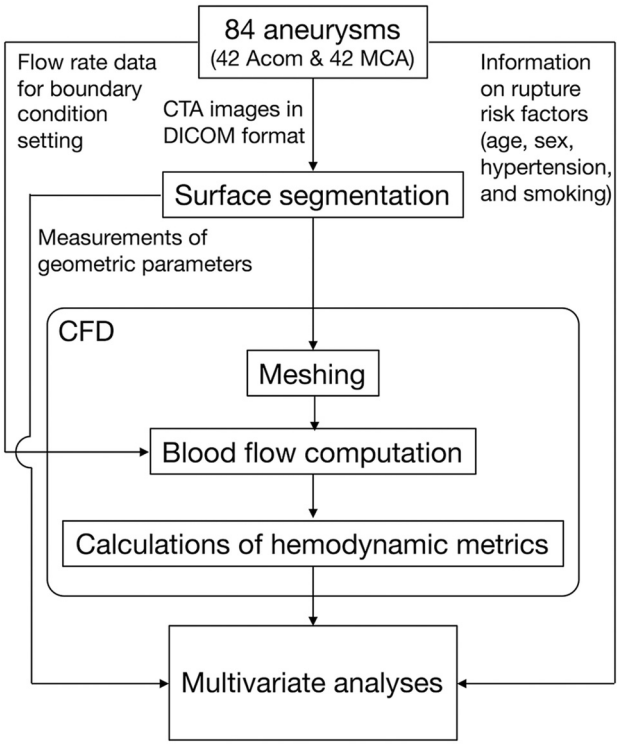

ON-LINE FIG 1. The flow chart of the methods used in this study.

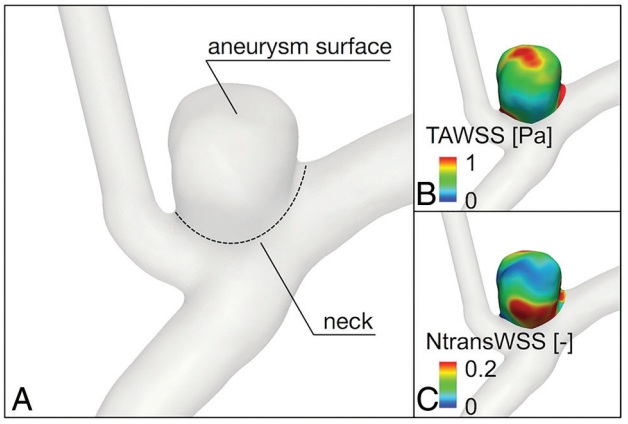

ON-LINE FIG 2. Hemodynamic metric reduction to compare aneurysm-specific values among the patients. *A*, The aneurysm neck was interactively delineated as seen in Cebral et al[10] to extract the aneurysm surface from the connected vessels. *B* and *C*, Examples of the extracted distributions of the hemodynamic metrics. Each metric was averaged over the aneurysm surface, and the values were then used for the statistical comparisons among the patients.

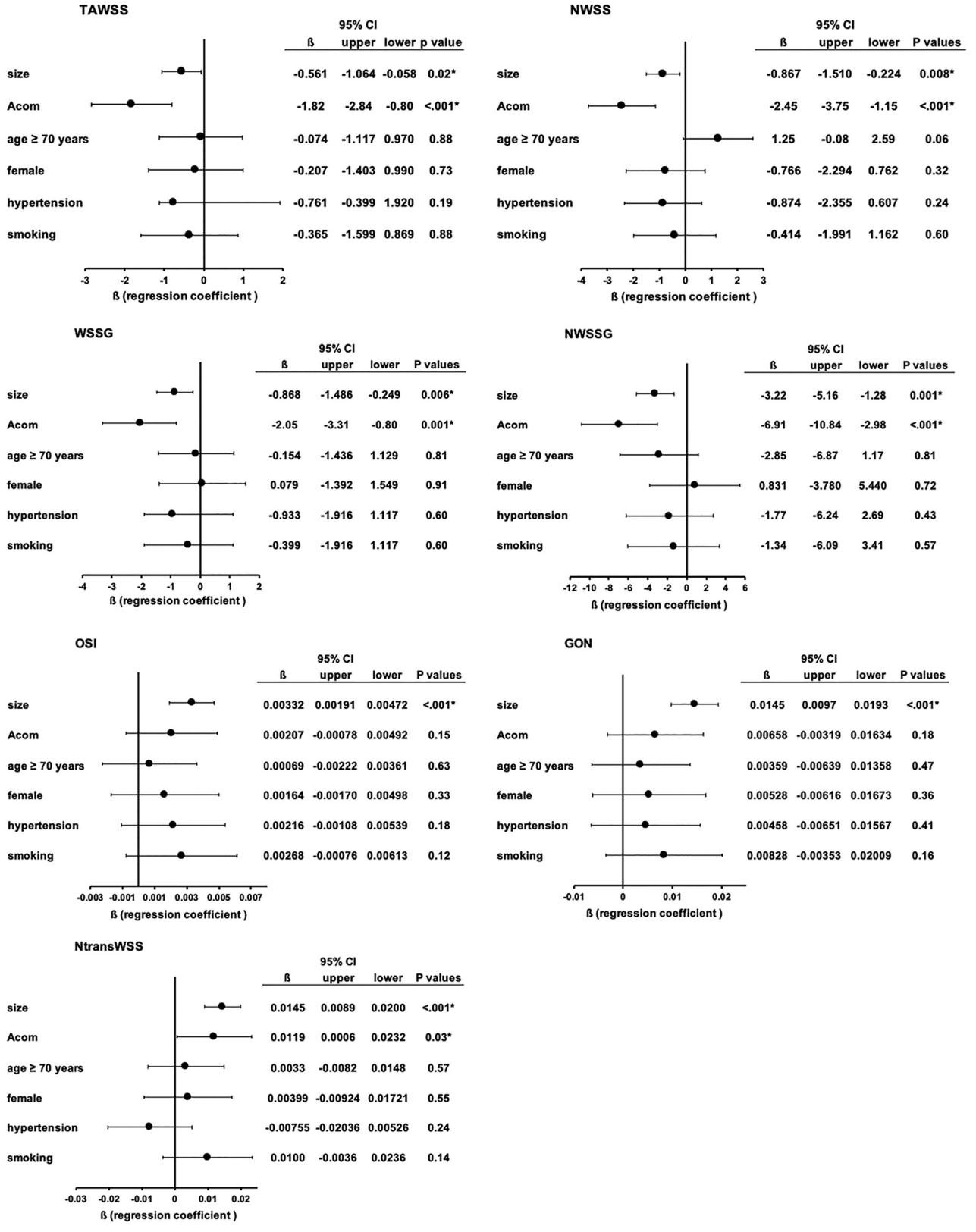

ON-LINE FIG 3. Forest plots showing the association of known rupture risk factors with hemodynamic metrics as assessed by multivariate regression analysis after adjustment for age (70 years or older), sex, hypertension, smoking history, location (AcomA and MCA aneurysms), and size. The *asterisk* indicates $P < .05$.

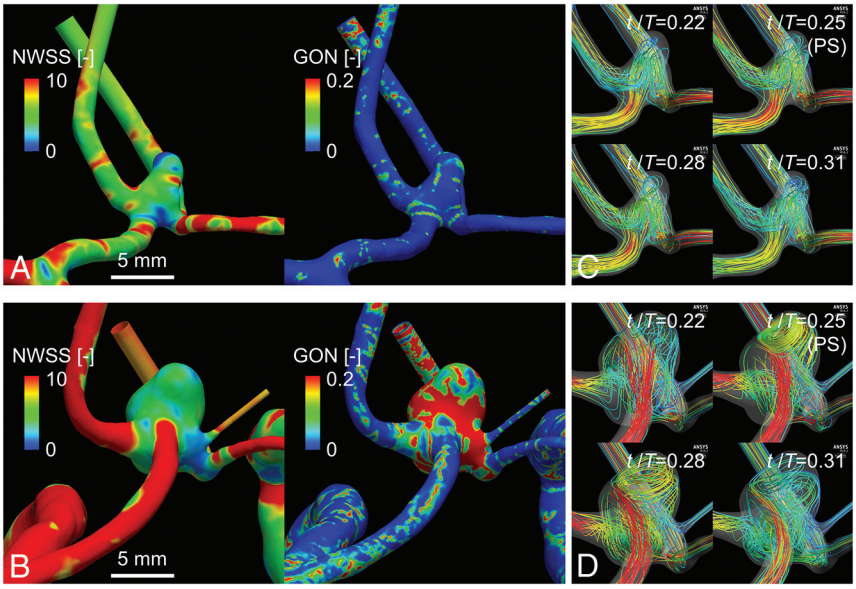

ON-LINE FIG 4. Comparisons of hemodynamic metrics and streamlines between a representative small aneurysm (*A* and *C*) and a large aneurysm (*B* and *D*). PS indicates peak systole.

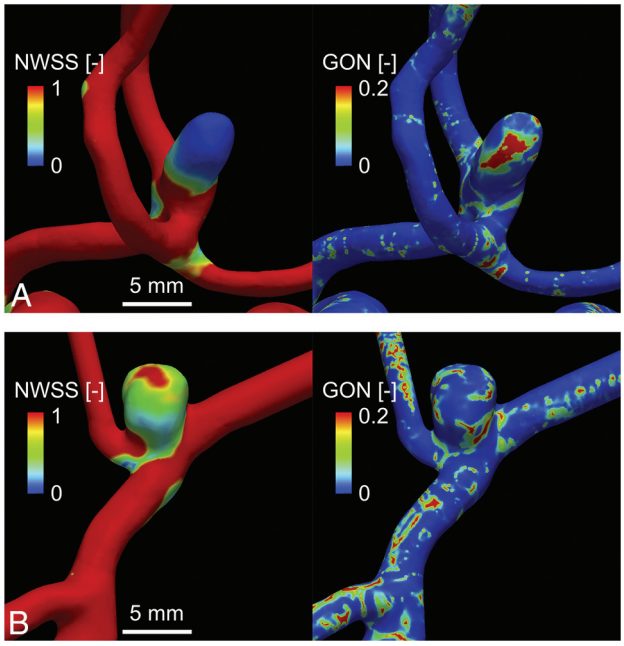

ON-LINE FIG 5. Comparisons of hemodynamic metrics between a representative anterior communicating artery aneurysm (*A*) and an MCA aneurysm (*B*).